Physics and Chemistry of Minerals (2021) 48:17
https://doi.org/10.1007/s00269-021-01139-5

ORIGINAL PAPER

High-pressure and high-temperature single-crystal X-ray diffraction of complex garnet solid solutions up to 16 GPa and 823 K

Christopher Beyer[1] · Alexander V. Kurnosov[2] · Tiziana Boffa Ballaran[2] · Daniel J. Frost[2]

Received: 13 November 2019 / Accepted: 1 March 2021 / Published online: 28 March 2021

Abstract

P–V–T equations of state (EoS) of synthetic garnet solid solutions with ternary grossular–almandine–pyrope compositions relevant to the Earth's upper mantle have been determined in order to examine whether garnet properties can be accurately interpolated from those of the end-members. Volumes have been measured as a function of pressure using single-crystal X-ray diffraction measurements performed inside a diamond anvil cell. Isothermal bulk moduli and first pressure derivatives were obtained by fitting the *P–V* data using a third-order Birch–Murnaghan equation of state. Two nominally eclogitic garnets ($Prp_{47}Alm_{19}Grs_{31}And_3$ and $Prp_{53}Alm_{19}Grs_{18}And_3Sps_7$) were found to have isothermal bulk moduli (K_{T0}) and pressure derivatives (K'_{T0}) of 170(3) GPa, 4.1 (4) and 173 (2) GPa, 3.8 (5), respectively. K_{T0} and K'_{T0} for an almandine-rich garnet ($Prp_{26}Alm_{63}Grs_6And_5$) were found to be 175 (3) GPa and 3.7 (7), respectively. High-temperature compression experiments at 703 K and 823 K were carried out on sample $Prp_{47}Alm_{19}Grs_{31}And_3$, resulting in the high-temperature EoS term $(\partial K_T/\partial T)_P = -0.025$ (6) and a thermal expansion (α_0) of 2.86 (4) $\times 10^{-5}$ K^{-1}. The results imply that the bulk moduli of aluminous garnet solid solutions stable at upper mantle conditions can be deduced from the properties of the end-members with minimal uncertainty. We show that the difference in the bulk sound velocity determined for a multicomponent eclogitic garnet composition and obtained for the same composition from the end-member properties is better than 0.5% for pressures and temperatures corresponding to Earth's upper mantle.

Keywords Garnet · X-ray diffraction · Equation of state · Earth's Mantle

Introduction

Garnet minerals usually crystallize in the cubic space group *Ia3d* and consist of a three-dimensional network of alternating corner-sharing tetrahedra and octahedra among which large distorted eightfold coordinated cubes reside. The general crystal-structural formula of garnet is $X_3^{[8]}Y_2^{[6]}Z_3^{[4]}O_{12}$, where *X* is the eightfold coordinated site mainly occupied by large divalent cations such as Mg, Ca, Fe^{2+}, or Mn^{2+}; *Y* is the octahedral site mainly occupied by medium size trivalent cations such as Al, Fe^{3+}, or Cr^{3+}, and *Z* is the tetrahedral site usually occupied by Si, although minor Fe^{3+} and H^+ may also substitute at this position. In the Earth's lower crust and shallow upper mantle, garnet is principally a solid solution of the end-members grossular, Grs ($Ca_3Al_2Si_3O_{12}$), almandine, Alm ($Fe_2^{3+}Al_2Si_3O_{12}$), and pyrope, Prp ($Mg_3Al_2Si_3O_{12}$), and it is volumetrically the most important Al-bearing phase down to the Earth's transition zone.

Given the abundance of garnet, seismic velocities of the Earth's upper mantle will depend in part on its elastic properties. Although end-member properties and binary systems of aluminous garnet solid solutions have been studied in some detail (e.g. Bass 1989; Pavese et al. 2001; Arimoto et al. 2015; Milani et al. 2017) (see also Supplementary Table A1), only a few studies have attempted to examine the elastic properties of more complex solid solutions (Duba and Olinger 1972; Babuška et al. 1978; O'Neill et al. 1989; Chai et al. 1997; Jiang et al. 2004; Xu et al. 2019), such as those representative of naturally occurring garnets found in mantle xenoliths. Moreover, only one study (Xu et al. 2019) has examined the compressibility of garnets expected to form from mafic, i.e. eclogitic bulk compositions in the mantle where Ca and Fe contents are higher and more variable

✉ Christopher Beyer
christopher.c.beyer@rub.de

[1] Ruhr-Universitat Bochum, Universitätsstr. 150, 44780 Bochum, Germany

[2] Bayerisches Geoinstitut,University of Bayreuth, 95440 Bayreuth, Germany

than those found in peridotite assemblages (e.g. Grütter et al. 2004; Kiseeva et al. 2013).

It is often assumed that the bulk modulus of an intermediate solid solution composition can be determined from the end-member bulk moduli using an averaging scheme involving either the mole fraction or volume fraction (Babuška et al. 1978; Jackson et al. 1978; Ita and Stixrude 1992). However, such relationships which assume a linear dependence of the bulk moduli with composition, in analogy to Vegard's law for volume dependence, have not been tested at high temperatures or with ternary solid solutions containing near equimolar proportions of components, for which any deviation from a linear averaging scheme might be expected to be the largest. Upper mantle eclogitic garnets, for example, are expected to have subequal proportions of Prp, Grs, and Alm components. Studies on garnet excess volumes of mixing (Berman and Koziol 1991; Mukhopadhyay et al. 1993; Ganguly et al. 1996; Geiger 2000) show very significant deviations from Vegard's law for numerous garnet solid solutions. The results of static compression and acoustic velocity measurements reported to date show large discrepancies among the values of K_0 and especially K'_0 reported in different studies (Supplementary Table A1). This is particularly the case for the Alm end-member and for Alm-rich samples (Supplementary Table A1), where reported bulk moduli vary between 159 and 185 GPa. It still remains an open question whether these inconsistencies arise from differences in experimental techniques, pressure-transmitting media, pressure ranges, or whether deviations from linear functions of end-member properties have a significant impact on the compressibility of garnets. An examination of the effect of garnet mixing behaviour on elastic properties is, therefore, important as such effects may influence accurate modelling of seismic velocities for mantle assemblages.

We have collected single-crystal X-ray diffraction data in a diamond anvil cell (DAC) at high pressure in order to obtain accurate values for the volume, isothermal bulk modulus (K_{T0}), and its first pressure derivative (K'_{T0}) for two garnet crystals with typical eclogitic compositions, as well as for one garnet with an Alm-rich composition, in order to quantify the effect of cation substitution on the elastic properties of ternary aluminous-garnet solid solutions. Moreover, we have performed a high-pressure and high-temperature study on one eclogitic garnet to shed light on whether elastic properties obtained using a linear interpolation of end-member components can reproduce those experimentally observed at high-pressure and high-temperature.

Methods

Syntheses and characterization of garnet single crystals

Synthetic glasses, produced from analytical grade oxides, hydroxides, and carbonates (compositions are given as oxides in Supplementary Table A2), were used as starting materials for the syntheses of large garnet crystals. The reagents were ground together in an agate mortar for approximately 30 min. Mixtures were calcinated at 1000 °C for 3 h and then fused at 1600 °C in an Fe-saturated Pt crucible for 1 h and subsequently quenched in water. The recovered glasses were reground, pressed into a pellet, and reduced in a gas-mixing furnace at 1000 °C with a mixture of CO–CO_2 set to an oxygen fugacity of approximately 2 log units below the fayalite–magnetite–quartz oxygen buffer (FMQ). The recovered material appeared glassy and homogeneous but could well have contained microcrystals. Two wt. % H_2O was then added to the starting glasses as $Al(OH)_3$, in order to promote the growth of large, inclusion-free, and homogeneous crystals. One starting material (for the H3605 synthesis) also contained 2 wt. % of F added as CaF_2. Glass powders were loaded into graphite capsules, sealed with graphite lids, and enclosed in Pt capsules, in order to limit the oxygen fugacity during the synthesis experiments to values below the $C + O_2 = CO_2$ (CCO) oxygen buffer. Two synthesis experiments (B834 and A719) were conducted at 3 GPa and 1500 °C in a piston-cylinder apparatus using a half-inch assembly with a talc-Pyrex sleeve. A tapered graphite furnace was used as a heater. The experiments were equilibrated at the run temperature for 24 h and then quenched by shutting off the electrical power. One synthesis experiment (H3605) was performed in a multi-anvil apparatus at 5.4 GPa and 1350 °C. A Cr-doped MgO octahedron with an edge length of 18 mm was used as a pressure medium. Pressure was generated with a Kawai-type multi-anvil press using 32-mm edge length tungsten carbide cubes with truncated corners of 11 mm edge length. The sample was heated with a stepped graphite heater for 60 min. The temperature was estimated based on a temperature-to-power calibration.

The recovered run products consisted of large prismatic garnet crystals with dimensions that were on average 70–100 μm in diameter together with quenched melt and, in the case of samples A719 and B834, omphacitic pyroxene crystals. The recovered garnet crystals from samples H3605 and A719 are colourless, whereas those from the Alm-rich sample B834 are slightly brown.

Chemical compositions of the garnet crystals (Table 1) were measured using a JEOL JXA-8200 microprobe

Table 1 Chemical compositions of garnet crystals

	H3605	A719	B834
SiO_2	40.7 (2)	39.7 (1)	38.2 (2)
TiO_2	0.5 (1)	056 (9)	0.27 (3)
Al_2O_3	21.9 (2)	23.2 (2)	21.8 (1)
FeO	9 (1)	9.0 (1)	27.65 (2)
Fe_2O_3*	1.11	1.11	1.62
MnO	0.22 (4)	3.59 (7)	n.a
MgO	12.5 (1)	14.4 (2)	6.4 (7)
CaO	12.7 (2)	8.01 (1)	3.57 (5)
Na_2O	0.25 (3)	0.07 (2)	n.a
$Fe^{3+}/\Sigma Fe$	0.10**	0.10 (4)	0.05 (1)
Normalized percentages of end-member components			
Pyrope	46.7	52.9	26.2
Almandine	18.8	18.5	63.3
Grossular	30.9	18.0	5.5
Andradite	3.1	3.1	5.0
Spessartine	0.5	7.5	
Total	100.0	100.0	100.0

The 1σ uncertainty based on at least 10 analyses is given in parentheses. Na and Ti were neglected in the calculation of the end-member components

n.a. not analysed

*Based on the $Fe^{3+}/\Sigma Fe$ ratio of measured Mössbauer spectra (see Supplementary Figures S1a,b)

**Inferred from sample A719, see text for details

(EMPA). Details of the standards employed and the measurement conditions are reported in Beyer et al. (2015). The compositions of samples H3605, A719, and B834 are described as solid solutions of Prp, Alm, and Grs, with minor amounts of andradite, And ($Ca_3Fe^{3+}_2Si_3O_{12}$), and spessartine, Sps ($Mn_3Al_2Si_3O_{12}$) (Table 1). Trace amounts of Na_2O and TiO_2 have been neglected in the calculation of the end-member components. The andradite component of samples B834 and A719 has been calculated from the $Fe^{3+}/\Sigma Fe$ ratio determined using Mössbauer spectroscopy (Table 1). The measured Mössbauer spectra are reported in Supplementary Figures S1a/b. It was not possible to collect a Mössbauer spectrum for sample H3605; therefore, its $Fe^{3+}/\Sigma Fe$ ratio has been assumed to be identical to that of sample A719, given their similar iron contents and the identical capsule material used for the synthesis. The resulting average compositions for the three garnets investigated in this study are the following: $(Mg_{1.40}Fe^{2+}_{0.56}Ca_{1.02}Mn^{2+}_{0.02})(Al_{1.94}Fe^{3+}_{0.06})Si_3O_{12}$, $Prp_{47}Alm_{19}Grs_{31}And_3$, for sample H3605; $(Mg_{1.58}Fe^{2+}_{0.56}Ca_{0.64}Mn^{2+}_{0.22})(Al_{1.94}Fe^{3+}_{0.06})Si_3O_{12}$, $Prp_{53}Alm_{19}Grs_{18}And_3Sps_7$, for sample A719, and $(Mg_{0.78}Fe^{2+}_{1.90}Ca_{0.32})(Al_{1.90}Fe^{3+}_{0.10})Si_3O_{12}$, $Prp_{26}Alm_{63}Grs_6And_5$ for sample B834.

Single-crystal X-ray data collection and structural refinements

Diffracted X-ray intensity data were collected for the three garnet single crystals using an Xcalibur diffractometer employing Mo Kα radiation selected with a graphite monochromator and operated at 50 kV and 40 mA, in conjunction with a CCD detector at a distance of 45 mm. Several ω scans were chosen to obtain coverage of the full reciprocal sphere up to $2\Theta_{max} = 72°$, with an exposure time of 15–60 s/frame depending on the crystal dimensions. Lorentz and polarization factors together with an empirical absorption correction were employed during the integration of the reflection intensities using the CrysAlis package (Oxford Diffraction 2006). The measured reflections for each data collection were consistent with the cubic space group $Ia\bar{3}d$. Structure refinements were performed based on F^2 using the SHELX97 program package (Sheldrick 2008) in the WingX system (Farrugia 1999) and starting from the atomic structural parameters of Prp reported by Zhang et al. (1998). Neutral scattering factors for Si, Al, Mg, Fe, Ca, and O were used, and all atoms were refined anisotropically. The tetrahedral site was considered fully occupied by Si, whereas the occupancies of Al and Fe^{3+} at the octahedral site were constrained to the values of the chemical analysis to account for the small amount of the andradite component (Table 1). The occupancies of Mg, Fe, and Ca at the X site were modelled as follows: the amount of Ca, XCa, was fixed according to the chemical analyses (Table 1), whereas the amounts of Mg and Fe, XMg and XFe, were refined with the constraint XMg + XFe + XCa = 1. In this way, it was possible to account for the small amount of the spessartine component by assuming the same scattering factor as Fe, which is very similar to that of Mn. Details of all data collections and structural refinements are reported in the deposited CIFs.

High-pressure and high-temperature compression experiments in a diamond anvil cell

One single crystal for each composition was selected for the diamond anvil cell (DAC) experiments on the basis of its optical properties, chemical homogeneity (Supplementary Figure S2), and sharp X-ray diffraction profiles. The chosen crystals were polished down to a thickness of 16–20 µm and cut into pieces with a maximum edge length of 80 µm. One crystal slice for each composition was then loaded into the sample chamber of a piston cylinder-type BX90 diamond anvil cell (Kantor et al. 2012) equipped with Boehler–Almax-type Ia diamonds (Boehler and De Hantsetters 2004) with 500 µm culets. The sample chamber was a 250-µm-diameter hole spark eroded into the centre of a Re gasket that had been pre-indented to a thickness of 50–70 µm. A neon pressure-transmitting medium was

loaded into the DAC sample chamber using a gas-loading device installed at the Bayerisches Geoinstitut (Kurnosov et al. 2008).

Room temperature compression experiments on crystals H3605 ($Prp_{47}Alm_{19}Grs_{31}And_3$) and B834 ($Prp_{26}Alm_{63}Grs_6And_5$) were performed using a Huber four-circle diffractometer equipped with Mo Kα radiation and a point detector. Room temperature compression experiments on crystal A719 ($Prp_{53}Alm_{19}Grs_{18}And_3Sps_7$) as well as the high-temperature/high-pressure experiments on crystal H3605 ($Prp_{47}Alm_{19}Grs_{31}And_3$) were performed using a Huber four-circle diffractometer in conjunction with a Rigaku FR-E + SuperBright rotating anode X-ray source (Mo Kα), equipped with multilayer VaryMax focusing optics (Trots et al. 2011).

High-pressure and room temperature unit-cell parameters (Table 2) were obtained using the 8-position centring method (King and Finger 1979) implemented in the SINGLE program (Angel and Finger 2011), employing at least 10 reflections for each crystal. No significant offsets between symmetry constrained and unconstrained unit-cell parameters were observed. The full-width at half-maximum (FWHM) of any reflection was smaller than 0.13° in ω scans that were performed at each pressure. To ensure the equilibration of the pressure and relaxation of the internal stresses, samples were left for periods of 24 h after each pressure increment before measurements were performed. The fluorescence shift of a ruby chip loaded together with the garnet sample was used to measure the pressure according to the calibration reported by Jacobsen et al. (2008).

An external resistance heater was made from an alumina ceramic cylinder, 7 mm high, 2 mm wall-thickness, and an inner diameter of 17 mm that was wrapped with 0.5-mm-diameter Pt wire. The heater was inserted around the seats of the diamond anvils for the high-temperature/high-pressure experiments. Temperatures within the cell were monitored with two PtRh S-type thermocouples (TC) positioned as close as possible to the gasket hole. To protect the diamonds from oxidation, the DAC was confined in a water-cooled stainless steel cell and flushed with a continuous stream of $Ar_{99}H_1$ gas during the measurements. *P–V–T* experiments were performed at 703 and 823 K on sample H3605 ($Prp_{47}Alm_{19}Grs_{31}And_3$) (H3605T1 and H3605T2). Due to spatial limitations caused by the heating setup, high-pressure and high-temperature unit-cell data were obtained from the centring of 4–6 reflections in four positions. For this reason, the overall precision of the unit-cell parameters measured at high-temperature (Table 3) is lower than that obtained for the *P–V* experiments. The volume of a single crystal of Sm:YAG (Sm-doped $Y_3Al_5O_{12}$), loaded together with the H3605 ($Prp_{47}Alm_{19}Grs_{31}And_3$) garnet crystal, was measured at each pressure/temperature point (Supplementary Table A3) and used to determine the pressure according to the *P–V–T* equation of state reported by Trots et al. (2013).

Table 2 Unit-cell volumes of garnet single crystals at high pressure and ambient temperature

H3605		A719		B834	
P [GPa]	*V* [Å^3]	*P* [GPa]	*V* [Å^3]	*P* [GPa]	*V* [Å^3]
1.0E−4	*1570.22 (28)*	1.0E−04	1554.84 (4)	1.0E−04	1542.42 (11)
0.44 (5)	1565.24 (1)	0.71 (5)	1548.55 (14)	1.02 (5)	1533.86 (10)
1.22 (5)	1557.88 (7)	1.36 (5)	1543.54 (1)	1.82 (10)	1527.12 (10)
1.76 (13)	1553.68 (7)	2.22 (5)	1536.22 (17)	2.69 (10)	1519.06 (8)
2.64 (5)	1545.66 (15)	3.39 (5)	1525.39 (14)	4.16 (10)	1507.86 (8)
3.45 (7)	1537.99 (11)	4.76 (5)	1514.45 (22)	4.84 (10)	1502.38 (10)
4.07 (5)	1533.21 (9)	5.69 (5)	1507.33 (8)	6.86 (10)	1485.85 (13)
5.15 (5)	1526.11 (11)	6.86 (5)	1498.4 (11)	7.99 (10)	1478.82 (13)
5.93 (10)	1519.18 (8)	7.99 (10)	1489.07 (14)	9.11 (5)	1470.93 (19)
7.17 (10)	1510.3 (8)	9.50 (5)	1479.14 (12)	9.72 (16)	1466.00 (18)
8.54 (5)	1498.6 (21)	10.52 (5)	1472.19 (16)	10.60 (5)	1460.61 (21)
10.93 (5)	1481.35 (17)			11.08 (5)	1456.78 (24)
13.1 (10)	1467.08 (17)				
13.97 (10)	1462.06 (14)				
14.53 (10)	1458.88 (16)				
15.39 (10)	1452.56 (15)				
15.72 (5)	1450.35 (16)				

Volumes in italics were not used in the equation of state refinement

The 1σ uncertainties are given in parentheses

P pressure, *V* volume

Table 3 Unit-cell lattice volumes measured at high pressure and high temperature for sample H3605

703 K		823 K	
P [GPa]	*V* [Å^3]	*P* [GPa]	*V* [Å^3]
1.0E−04	1591.15 (5)	1.0E−04	1598.16 (5)
2.18 (10)	1570.10 (4)	5.60 (10)	1543.70 (30)
2.33 (10)	1568.33 (63)	8.25 (10)	1523.97 (48)
2.41 (10)	1567.32 (27)	9.10 (10)	1515.79 (12)
2.84 (10)	1564.29 (53)	9.60 (10)	1511.2 (1.1)
3.25 (10)	1561.00 (75)	10.30 (10)	1505.47 (82)
3.85 (10)	1553.93 (19)		
6.34 (10)	1532.74 (77)		

The 1σ uncertainties are given in parentheses. The pressures are based on the EoS of YAG (see supplementary Table A3)

Results

Garnet crystal chemistry

Structural refinements of the three samples investigated in this study gave rise to a set of precise bond distances for the three different cation sites of the garnet structure (see deposited CIFs). Neglecting the small amount of And, the main cation substitution in these samples occurs at the X-site; we can, therefore, expect that the chemical variation has a primary effect on the two non-equivalent X–O bond distances, X(1)–O and X(2)–O, and the X site distortion. However, since each $[XO]_8$ site shares edges with four other distorted cubes, with four octahedra and with two tetrahedra (so that only 2 of its 12 edges are unshared), any chemical change at the X-site will also affect the geometry of the other two polyhedra. The variations with Grs content of the two crystallographically independent X-O bond lengths are shown in Fig. 1. Both X–O bond lengths increase with increasing Grs content and samples belonging to the Prp—Grs binary join (Ganguly et al. 1993) lie very close to the line uniting the end-member values, with minor deviation from linearity. Substitution of Mg for Fe^{2+} along the Prp—Alm join (Armbruster et al. 1992) also gives rise to a linear increase of the X-O bond lengths, albeit smaller. The ternary Prp—Grs—Alm garnets investigated in this study and the natural samples investigated by Quartieri et al. (1995) have X–O bond lengths that follow more closely the Alm—Grs linear trend, even though some of these samples have relatively low Alm contents. This is particularly the case for the X(2)–O distance for which the samples from this study follow the Alm—Grs trend regardless of whether they contain 19% or 63% Alm. This implies that these distances cannot be adequately described by a linear interpolation between the end-member X–O bond distances.

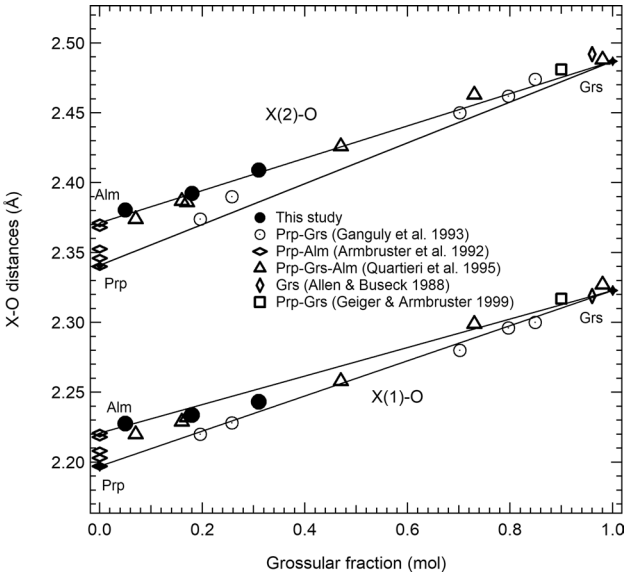

Fig. 1 Variation of the two non-equivalent X-O bond distances as a function of Grs mole fraction. Solid lines join the end-members Prp—Grs and Alm—Grs. Distances for Prp are taken from Meagher (1975), for Grs from Rodehorst et al. (2002), and for Alm from Armbruster et al. (1992). Data from this study are shown along with previous studies in both binary and ternary systems

A simple way to describe the distortion of the $[XO]_8$ polyhedron is by using the difference between the two non-equivalent X–O bond lengths, Δ(X–O). Ungaretti et al. (1995) have shown, on the basis of the crystal-chemical characterization of 281 natural garnets, that this value follows a trend which has a sharp change in slope at high Ca contents. Garnets in the Prp—Grs—Alm system follow this trend, and the variation in Δ(X–O) (Fig. 2) deviates significantly from the linear relation connecting the end-members. This implies that the local coordination around the X-site cations in ternary systems is substantially different from that around the same cations in the respective end-members, as noted for a $Grs_{90}Prp_{10}$ sample studied by Geiger and Ambruster (1999). The change in Δ(X–O) appears to mimic the excess volume of the Grs—Prp garnet solid solution (cf. Bosenick and Geiger 1997), implying that the distortion of the X-site may be responsible for this excess property.

Room temperature static compression experiments

Samples H3605 ($Prp_{47}Alm_{19}Grs_{31}And_3$), A719 ($Prp_{53}Alm_{19}Grs_{18}And_3Sps_7$), and B834 ($Prp_{26}Alm_{63}Grs_6And_5$) were compressed at room temperature up to 15.72, 10.52, and 11.08 GPa, respectively. The variation of the unit-cell volumes as a function of pressure (Table 2) is shown for each crystal in Fig. 3. The *P*–*V* compression data sets were fitted with a third-order Birch–Murnaghan equation of state (BM3-EoS) using the Eosfit7c

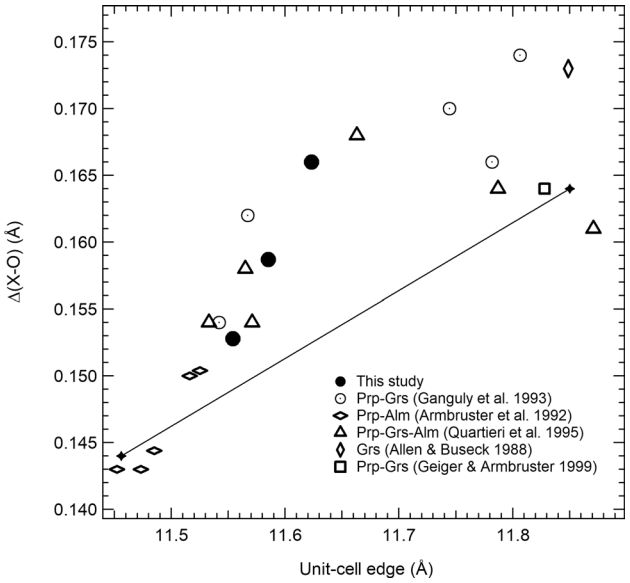

Fig. 2 The difference between the two non-equivalent X–O bond distances of the garnet structure as a function of the garnet unit-cell edge. The solid line joins the end-members Prp (Meagher 1975) and Grs (Rodehorst et al. 2002). The variation in this difference mirrors, to some extent, the excess volume of mixing observed in this system (cf. Bosenick and Geiger 1997) implying a common origin

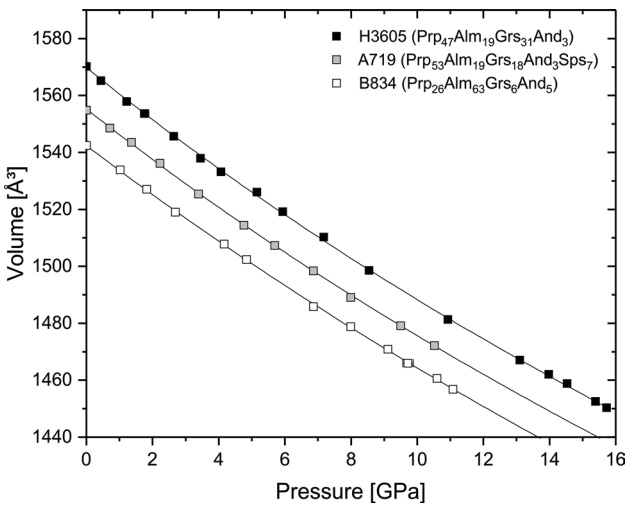

Fig. 3 Variation as a function of pressure of the unit-cell volumes of the garnets investigated in this study normalized with respect to the room pressure volume V_0. Uncertainties are generally smaller than the size of the symbols. Solid curves show the BM3-EoS fits to the *P–V* data

software package (Angel et al. 2014). For sample H3605 ($Prp_{47}Alm_{19}Grs_{31}And_3$), the volume measured at room pressure was not included in the fitting, since the crystal offset obtained from the measured reflections was not constant, indicating that there was a slight movement of the crystal inside the DAC between the room and high-pressure

Table 4 EoS parameters obtained from fitting the garnet single-crystal *P–V* data using a BM3-EoS

Sample	Composition	V_{T0} [Å^3]	K_{T0} [GPa]	K'_{T0}
H3605	$Prp_{47}Alm_{19}Grs_{31}And_3$	1569.2 (5)	170 (3)	4.1 (4)
A719	$Prp_{53}Alm_{19}Grs_{18}And_3Sps_7$	1554.85 (4)	173 (2)	3.8 (5)
B834	$Prp_{26}Alm_{63}Grs_6And_5$	1542.43 (11)	175 (3)	3.7 (7)

1σ uncertainties, expressed in terms of least units cited, in parentheses

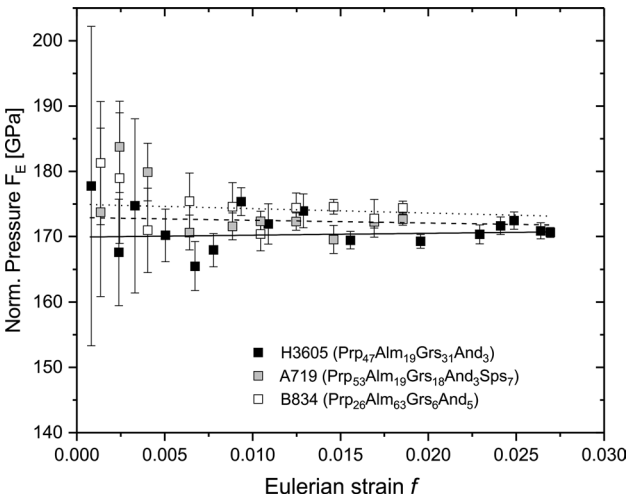

Fig. 4 Normalized pressure, F_E, as a function of Eulerian strain, f, for the room pressure compression data of the three garnets investigated in this study. Error bars represent propagated experimental uncertainties (Heinz and Jeanloz 1984). Dotted and solid lines are weighed linear fits through each dataset

measurements. The resulting EoS parameters are reported in Table 4.

To obtain an initial estimate of the magnitude of K'_{T0}, the Eulerian strains $f=[(V_0/V)^{(2/3)}-1]/2$ were plotted against the normalized pressure $F_E=P(3f(1+2))^{(5/2)}$ (Angel 2000) (Fig. 4). For all three garnets, the f—F_E plots suggest values of K'_{T0} close to 4, in agreement with a number of previous studies on garnets from the same system (Chai et al. 1997; Zhang et al. 1998, 1999; Sinogeikin and Bass 2000; Chantel et al. 2016; Xu et al. 2019; see also Supplementary Table A1). In a few instances, K'_{T0} values have been reported that are significantly larger than 4; however, as it can be seen in Supplementary Table A1, these appear to be outliers that may well be attributed to the use of particular pressure scales (e.g. Milani et al. 2015). The room temperature compressibilities of the garnets investigated in this study (Table 4) are very similar in spite of their different compositions with bulk moduli ranging between 170 (3) GPa, for the Grs-rich sample $Prp_{47}Alm_{19}Grs_{31}And_3$, to 175 (3) GPa for the Alm-rich sample $Prp_{26}Alm_{63}Grs_6And_5$. This is in broad

agreement with several experimental and ab initio studies that support the aluminous garnet compressibility scheme Grs > Prp > Alm, although several studies report outliers to this trend (Supplementary Table A1).

High-temperature static compression experiments

The variation with pressure of the unit-cell volumes collected during two high-temperature runs for sample H3605 ($Prp_{47}Alm_{19}Grs_{31}And_3$), which are labelled H3605T1 (703 K) and H3605T2 (823 K) (Table 3), is shown in Fig. 5. The entire *P–V–T* data set for this sample was fitted using a BM3-EoS combined with the thermal pressure expression based on the Einstein function described in Holland and Powell (2011) and implemented in the program EosFit7c (Angel et al. 2014). The Einstein temperature, Θ_E, was calculated according to the approximation described by Holland and Powell (2011):

$$\Theta_E = 10636/(S/n + 6.44) = 475 \text{ K}, \quad (1)$$

where S is the room temperature molar entropy and n is the number of atoms per formula unit. The value of $S = 318.6$ J K^{-1} mol^{-1} for the solid solution was obtained following the procedure described in Holland and Powel (2011). The resulting *P–V–T* EoS parameters are given in Table 5 and show a marginally lower value of K_{T0} for a slightly larger V_{T0} (1569.6 (3) Å^3) but still within errors of the values obtained from the room temperature fit (Table 4).

Using the high-temperature isothermal compression data for sample H3605 ($Prp_{47}Alm_{19}Grs_{31}And_3$), we have also calculated the temperature derivative of the bulk modulus, $(\partial K_T/\partial T)_P$, applying the linear relationship (e.g. Angel 2000):

$$K_T(T) = K_T(T_0) + (T - T_0)/(\partial K_T/\partial T)_P, \quad (2)$$

where T_0 is the reference temperature of 298 K. The resulting $(\partial K_T/\partial T)_P$ is − 0.025 (6) and is slightly larger than the values reported for Prp and Grs end-members, but significantly smaller than the value reported for the Alm end-member (Table 5).

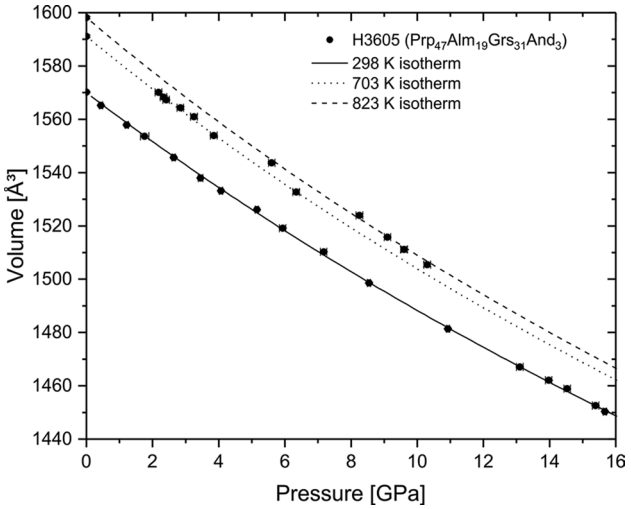

Fig. 5 Variations with pressure of the unit-cell volume of sample H3605 ($Prp_{47}Alm_{19}Grs_{31}And_3$) at room temperature and along two isotherms at 703 K and 823 K. Error bars are 1σ uncertainties

Discussion

Garnet compressibility

The compressibility of aluminous garnet end-members and solid solutions within the Prp—Grs—Alm system

Table 5 Thermoelastic parameters of aluminous garnets

Composition	K_{T0} [GPa]	K'_{T0}	$(\partial K_T/\partial T)_P$	α_0 [10^{-5} K^{-1}]	References
$Prp_{47}Alm_{19}Grs_{31}And_3$	167 (2)	4.4 (2)	− 0.025 (6)	2.86 (4)	1
$Prp_{73}Alm_{16}And_4Uv_6$	169.4 (8)	4.0 (7)	− 0.025 (1)		2
$Prp_{14}Alm_{62}Grs_{19}And_3Sps_2$	159.0 (9)	5.0 (2)	− 0.010 (4)	1.7 (2)	10
$Prp_{28}Alm_{38}Grs_{33}Sps_1$	162 (1)	4.3 (2)	− 0.010 (7)	3.5 (4)	10
Grs_{100}	166.57 (17)	4.96[a]	− 0.020 (1)	2.09 (2)	3, $(\partial K_T/\partial T)_P$ from 8
Prp_{100}	163.7 (1.7)	6.4 (4)		2.543 (5)	9
Prp_{100}	167 (3)	4.6[a]	− 0.021 (1)	2.89 (33)	4
Prp_{100}	169.4 (2.0)		− 0.019 (3)		5
$Alm_{86}Prp_7Sps_7$	177 (2)	4[a]	− 0.032 (16)	3.1 (7)	6
Alm_{100}	179 (3)	4[a]	− 0.043 (14)	2.6 (5)	7

[a]Fixed

1: this study H3605 BM3-EoS + Holland and Powell (2011) thermal pressure, 2: Suzuki and Anderson (1983), 3: Milani et al. (2017), 4: Zou et al. (2012), 5: Sinogeikin and Bass (2000), 6: Fan et al. (2009), 7: Arimoto et al. (2015), 8: Isaak et al. (1992), 9: Milani et al. (2015), and 10: Xu et al. (2019)

has been studied extensively by means of a wide range of techniques. The majority of bulk moduli reported in the literature (Supplementary Table A1) vary between 165 and 175 GPa. Compared to this range, only a few studies stand out because they report K_{T0} values which are either significantly larger, e.g. Zhang et al. (1999) report 185 (3) GPa for Alm, or smaller, e.g. Du et al. (2015) and Xu et al. (2019) report values in the range 160 (2) GPa for Prp—Grs and Prp—Grs—Alm solid solutions, respectively. These inconsistencies cannot be attributed to obvious chemical variations and are, therefore, hard to include in a consistent scheme of aluminous garnet compressibility. Furthermore, although values of K'_{T0} show some scatter, the majority of studies point toward a bulk modulus derivative close to four, as obtained in this study. The very similar values of K_{T0} and K'_{T0} obtained for the garnets studied here (Table 4) indicate quite strongly that cation substitution at the garnet X-site has little to no resolvable effect on the compressibility, despite more significant effects on the excess volume of mixing. The octahedral–tetrahedral framework is primarily responsible for the compression behaviour of garnet, as implied by the lower bulk modulus of 157.4 (3) GPa reported for skiagite garnet, where Fe^{3+} occupies the octahedral site (Woodland et al. 1999) or the value of 161.7 (20) GPa obtained for a majorite-rich garnet where 80% of Mg and Si occupy the octahedral site (Sinogeikin and Bass 2002). Similarly, ab initio calculations (Milman et al. 2001) give a smaller K_{T0} value for the end-member andradite with respect to aluminous garnets end-members; note, however, that the cation substitution at the octahedral site needs to be substantial before any effect will be observed, since up to 5 mol% of And component appears to have little effect on the bulk modulus of the Alm-rich garnet B834 ($Prp_{26}Alm_{63}Grs_6And_5$) investigated in this study.

The few thermoelastic parameters of aluminous garnet solid solutions present in the literature (Sumino and Nishizawa 1978; Suzuki and Anderson 1983; Isaak et al. 1992; Xu et al. 2019) reveal a range of $(\partial K_T/\partial T)_P$ values that is larger than the experimental uncertainties (Table 5). In order to infer whether there is a compositional dependence, we have compared the $(\partial K_T/\partial T)_P$ obtained in this study with those reported for the end-members Prp (Zou et al. 2012), Alm (Fan et al. 2009; Arimoto et al. 2015) and Grs (Isaak et al. 1992) (Fig. 6). The samples investigated in this study and that investigated by Suzuki and Anderson (1983) lie close to the Prp and Grs curves. The only significant difference is shown by the Alm end-member, which has a lower $(\partial K_T/\partial T)_P = -0.043$ (14). The sample studied by Fan et al. (2009), containing a larger amount of Alm than that present in our sample, also lies closer to the Alm trend in Fig. 6. This implies that Alm has the most significant effect on the softening of the bulk modulus at high temperatures, in spite of giving the stiffest room pressure compressibility. The recent data of Xu et al. (2019) that report higher values of $(\partial K_T/\partial T)_P$ are clearly inconsistent with these results.

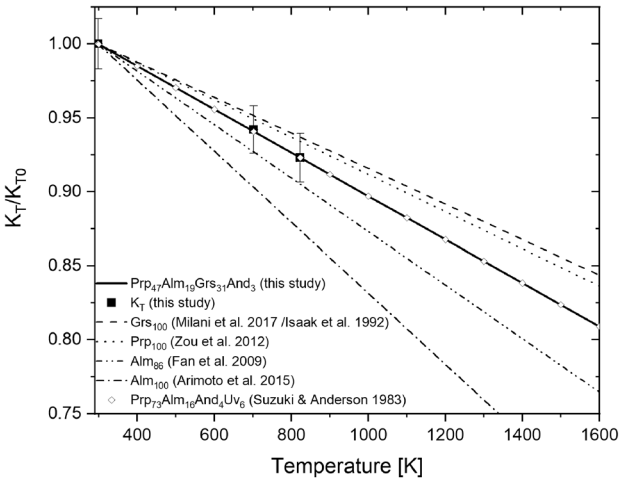

Fig. 6 Variation of the K_T/K_{T0} ratio with temperature for sample H3605 ($Prp_{47}Alm_{19}Grs_{31}And_3$). Error bars indicate the 1σ uncertainty, with σ_{max} being approximately 3%. Note that the data of Suzuki and Anderson (1983) overlap almost perfectly with our data and have a similar Alm content, although a quite different Grs content. The solid curve is calculated using the EoS data from this study given in Table 5

Calculation of garnet elastic properties at upper mantle conditions

Garnets formed within peridotite compositions have Grs and Alm contents that are sufficiently small that their thermoelastic properties are unlikely to be significantly different from Prp. Garnets produced within mantle eclogites, on the other hand, can have Grs and Alm amounts up to 80% and 90%, respectively (e.g. Schulze et al. 2000; Schulze 2003; Grütter et al. 2004). The garnet composition expected to form from an average MORB composition in the upper mantle would contain approximately 30% Grs and Alm (e.g. Aoki and Takahashi 2004). The data collected in this study can provide a quantitative assessment of whether the elastic properties interpolated from linear mixing of end-member component properties can reproduce the actual behaviour of a ternary garnet.

The bulk sound velocity of sample H3605 ($Prp_{47}Alm_{19}Grs_{31}And_3$) has been calculated at the highest experimental temperature (823 K) and at 1473 K according to the following expression:

$$\Phi = \sqrt{K_S/\rho}, \quad (3)$$

where ρ is the density extrapolated to high-pressures and temperatures using the EoS parameters of Table 5. K_S is the

isentropic bulk modulus calculated from the isothermal bulk modulus according to Anderson and Isaak (1995):

$$K_S = K_T(1 + \alpha\gamma T), \tag{4}$$

where α is the thermal expansion coefficient of sample H3605 ($Prp_{47}Alm_{19}Grs_{31}And_3$) (Table 5) and γ is the Grüneisen parameter, for which we use the room pressure value of 1. The chosen value is consistent with estimates for all three end members (Stixrude and Lithgow-Bertelloni 2011) and is not expected to change significantly over the pressure range explored.

In Fig. 7 we compare the experimentally determined bulk sound velocity calculated for sample H3605 ($Prp_{47}Alm_{19}Grs_{31}And_3$), with a calculation for the same composition made using the EoS and end-member parameters from Stixrude and Lithgow-Bertelloni (2011) and the Reuss averaging scheme

$$K_{ss} = \sum_{i=1}^{n} v_i K_i, \tag{5}$$

where v_i is the partial molar volume and K_i the bulk modulus of the end-member i. The first observation is that at 823 K, the maximum temperature reached in the experimental measurements, the difference between the bulk sound velocity calculated from our experimental results and that obtained from the end-member model is very small (<0.5%) and decreases with increasing pressure. For a mantle potential temperature of 1473 K, the match between the extrapolated experimental bulk sound velocity and that determined using the end-member based model is still good although below 5 GPa a discrepancy develops towards lower pressure. This discrepancy, however, is caused by the different forms of the equations of state used and not from the averaging scheme employed in the model based on the end-member properties.

We conclude that, after resolving inconsistencies in the end-member values of K'_{T0} for Alm and Grs which appear to be close to four instead of having much larger values, linear averaging schemes of end-member thermoelastic properties provide a good approximation for the properties of multi-component aluminous garnets at conditions applicable to the Earth's upper mantle.

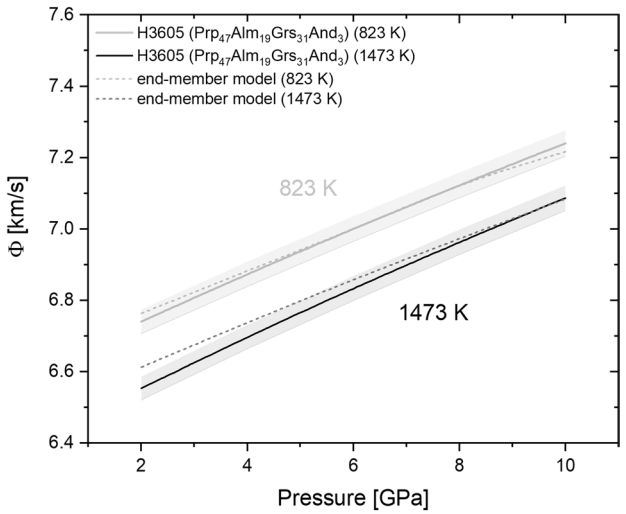

Fig. 7 Bulk sound velocity Φ calculated along isotherms at 823 K and 1473 K over a range of upper mantle pressures. The solid lines depict bulk sound velocities calculated from the EoS parameters fitted to sample H3605 ($Prp_{47}Alm_{19}Grs_{31}And_3$) and given in Table 5. The dashed lines show bulk sound velocities calculated using a linear average (Reuss averaging scheme) of garnet end-member properties determined for the H3605 composition from the EoS of Stixrude and Lithgow-Bertelloni (2005, 2011). The shaded areas indicate uncertainties of ±0.5%

Supplementary Information The online version contains supplementary material available at https://doi.org/10.1007/s00269-021-01139-5.

Acknowledgements This work was supported by the Deutsche Forschungsgemeinschaft (DFG) Grant No. FR1555-9 and European Research Council (ERC) Grant No. 227893 "DEEP" to D.J. Frost. We thank C. McCammon for her help with the collection of the Mössbauer spectra. C.B. thanks R. Myhill and an anonymous reviewer that helped to improve the manuscript considerably. We are indebted to members of the mechanical, electronics, and polishing workshop at the BGI for their efforts in maintaining the laboratory equipment.

Funding Open Access funding enabled and organized by Projekt DEAL.

References

Allen FM, Buseck PR (1988) XRD, FTIR, and TEM studies of optically anisotropic grossular garnets. Am Miner 73:568–584

Anderson OL, Isaak DG (1995) Elastic constants of mantle minerals at high temperature. Miner Phys Crystallogr Handb Phys Constants 2:64–97

Angel RJ (2000) Equations of state. Rev Miner Geochem 41:35–59

Angel RJ, Finger LW (2011) SINGLE: a program to control single-crystal diffractometers. J Appl Crystallogr 44:247–251. https://doi.org/10.1107/S0021889810042305

Angel RJ, Alvaro M, Gonzalez-Platas J (2014) EosFit7c and a Fortran module (library) for equation of state calculations. Zeitschrift für

Kristallographie Crystalline Materials 229:405. https://doi.org/10.1515/zkri-2013-1711
Aoki I, Takahashi E (2004) Density of MORB eclogite in the upper mantle. Phys Earth Planet Inter 143:129–143. https://doi.org/10.1016/j.pepi.2003.10.007
Arimoto T, Gréaux S, Irifune T, Zhou C, Higo Y (2015) Sound velocities of $Fe_3Al_2Si_3O_{12}$ almandine up to 19 GPa and 1700 K. Phys Earth Planet Inter 246:1–8. https://doi.org/10.1016/j.pepi.2015.06.004
Armbruster T, Geiger CA, Lager GA (1992) Single-crystal X-ray structure study of synthetic pyrope almandine garnets at 100 and 293 K. Am Miner 77:512–521
Babuška V, Fiala J, Kumazawa M, Ohno I, Sumino Y (1978) Elastic properties of garnet solid-solution series. Phys Earth Planet Inter 16:157–176. https://doi.org/10.1016/0031-9201(78)90086-9
Bass JD (1989) Elasticity of grossular and spessartite garnets by Brillouin spectroscopy. J Geophys Res Solid Earth 94:7621–7628. https://doi.org/10.1029/JB094iB06p07621
Berman RG, Koziol AM (1991) Ternary excess properties of grossular—pyrope—almandine garnet and their influence in geothermobarometry. Am Miner 76:1223–1231
Beyer C, Frost DJ, Miyajima N (2015) Experimental calibration of a garnet–clinopyroxene geobarometer for mantle eclogites. Contrib Miner Petrol 169:1–21. https://doi.org/10.1007/s00410-015-1113-z
Boehler R, De Hantsetters K (2004) New anvil designs in diamond-cells. High Press Res 24:391–396
Bosenick A, Geiger CA (1997) Powder X ray diffraction study of synthetic pyrope-grossular garnets between 20 and 295 K. J Geophys Res Solid Earth 102:22649–22657
Chai M, Brown JM, Slutsky LJ (1997) The elastic constants of a pyrope-grossular-almandine garnet to 20 GPa. Geophys Res Lett 24:523–526. https://doi.org/10.1029/97gl00371
Chantel J, Manthilake GM, Frost DJ, Beyer C, Ballaran TB, Jing Z, Wang Y (2016) Elastic wave velocities in polycrystalline $Mg_3Al_2Si_3O_{12}$-pyrope garnet to 24 GPa and 1300 K. Am Miner 101:991–997. https://doi.org/10.2138/am-2016-5335
Diffraction O (2006) CrysAlis Software system, Version 171.35. 19. Oxford Diffraction Ltd., Xcalibur CCD system
Du W, Clark SM, Walker D (2015) Thermo-compression of pyrope-grossular garnet solid solutions: non-linear compositional dependence. Am Miner 100:215–222
Duba A, Olinger B (1972) Compression of garnet to 100 kilobars. J Geophys Res 77:2496–2499
Fan DW, Zhou WG, Liu CQ, Liu YG, Wan F, Xing YS, Liu J, Bai LG, Xie HS (2009) The thermal equation of state of $(Fe_{0.86}Mg_{0.07}Mn_{0.07})_3Al_2Si_3O_{12}$ almandine. Miner Mag 73:95–102. https://doi.org/10.1180/minmag.2009.073.1.95
Farrugia LJ (1999) WinGX suite for small-molecule single-crystal crystallography. J Appl Crystallogr 32:837–838
Ganguly J, Cheng WJ, O'Neill HS (1993) Syntheses, volume, and structural changes of garnets in the pyrope-grossular join—implications for stability and mixing properties. Am Miner 78:583–593
Ganguly J, Cheng WJ, Tirone M (1996) Thermodynamics of aluminosilicate garnet solid solution: new experimental data, an optimized model, and thermometric applications. Contrib Miner Petrol 126:137–151. https://doi.org/10.1007/s004100050240
Geiger CA (2000) Volumes of mixing in aluminosilicate garnets: solid solution and strain behavior. Am Miner 85:893–897
Geiger CA, Armbruster T (1999) The crystal structure of a garnet solid solution $(Ca_{0.9}Mg_{0.1})_3Al_2[SiO_4]_3$ at 295 K and 100 K: Local site behaviour—dynamic and static disorder. Z Kristallogr 214:211–215
Grütter HS, Gurney JJ, Menzies AH, Winter F (2004) An updated classification scheme for mantle-derived garnet, for use by diamond explorers. Lithos 77:841–857. https://doi.org/10.1016/j.lithos.2004.04.012
Heinz DL, Jeanloz R (1984) The equation of state of the gold calibration standard. J Appl Phys 55:885–893
Holland TJB, Powell R (2011) An improved and extended internally consistent thermodynamic dataset for phases of petrological interest, involving a new equation of state for solids. J Metamorph Geol 29:333–383
Isaak DG, Anderson OL, Oda H (1992) High-temperature thermal expansion and elasticity of calcium-rich garnets. Phys Chem Miner 19:106–120
Ita J, Stixrude L (1992) Petrology, elasticity, and composition of the mantle transition zone. J Geophys Res Solid Earth 97:6849–6866
Jackson I, Liebermann RC, Ringwood AE (1978) The elastic properties of $(Mg_xFe_{1-x})O$ solid solutions. Phys Chem Miner 3:11–31. https://doi.org/10.1007/BF00357444
Jacobsen SD, Holl CM, Adams KA, Fischer RA, Martin ES, Bina CR, Lin JF, Prakapenka VB, Kubo A, Dera P (2008) Compression of single-crystal magnesium oxide to 118 GPa and a ruby pressure gauge for helium pressure media. Am Miner 93:1823–1828
Jiang FM, Speziale S, Duffy TS (2004) Single-crystal elasticity of grossular- and almandine-rich garnets to 11 GPa by Brillouin scattering. J Geophys Res Solid Earth. https://doi.org/10.1029/2004jb003081
Kantor I, Prakapenka VB, Kantor A, Dera P, Kurnosov A, Sinogeikin S, Dubrovinskaia N, Dubrovinsky L (2012) BX90: A new diamond anvil cell design for X-ray diffraction and optical measurements. Rev Sci Instrum 83:125102
King H, Finger L (1979) Diffracted beam crystal centering and its application to high-pressure crystallography. J Appl Crystallogr 12:374–378
Kiseeva ES, Litasov KD, Yaxley GM, Ohtani E, Kamenetsky VS (2013) Melting and phase relations of carbonated eclogite at 9–21 GPa and the petrogenesis of alkali-rich melts in the deep mantle. J Petrol 54:1555–1583. https://doi.org/10.1093/petrology/egt023
Kurnosov A, Kantor I, Boffa-Ballaran T, Lindhardt S, Dubrovinsky L, Kuznetsov A, Zehnder BH (2008) A novel gas-loading system for mechanically closing of various types of diamond anvil cells. Rev Sci Instrum 79:045110. https://doi.org/10.1063/1.2902506
Meagher EP (1975) The crystal structures of pyrope and grossularite at elevated temperatures. Am Miner 60:218–228
Milani S, Nestola F, Alvaro M, Pasqual D, Mazzucchelli ML, Domeneghetti MC, Geiger CA (2015) Diamond-garnet geobarometry: the role of garnet compressibility and expansivity. Lithos 227:140–147
Milani S, Angel RJ, Scandolo L, Mazzucchelli ML, Ballaran TB, Klemme S, Domeneghetti MC, Miletich R, Scheidl KS, Derzsi M, Tokár K, Prencipe M, Alvaro M, Nestola F (2017) Thermo-elastic behavior of grossular garnet at high pressures and temperatures. Am Miner 102:851–859
Milman V, Akhmatskaya EV, Nobes RH, Winkler B, Pickard CJ, White JA (2001) Systematic ab initio study of the compressibility of silicate garnets. Acta Crystallogr B 57:163–177
Mukhopadhyay B, Basu S, Holdaway MJ (1993) A discussion of margules-type formulations for multicomponent solutions with a generalized approach. Geochim Cosmochim Acta 57:277–283. https://doi.org/10.1016/0016-7037(93)90430-5
O'Neill B, Bass JD, Smyth JR, Vaughan MT (1989) Elasticity of a grossular-pyrope-almandine garnet. J Geophys Res Solid Earth 94:17819–17824. https://doi.org/10.1029/JB094iB12p17819
Pavese A, Levy D, Pischedda V (2001) Elastic properties of andradite and grossular, by synchrotron X-ray diffraction at high pressure conditions. Eur J Miner 13:929–937. https://doi.org/10.1127/0935-1221/2001/0013/0929

Quartieri S, Chaboy J, Merli M, Oberti R, Ungaretti L (1995) Local structural environment of calcium in garnets: a combined structure-refinement and XANES investigation. Phys Chem Miner 22:159–169

Rodehorst U, Geiger CA, Armbruster T (2002) The crystal structures of grossular and spessartine between 100 and 600 K and the crystal chemistry of grossular-spessartine solid solutions. Am Miner 87:542–549

Schulze DJ (2003) A classification scheme for mantle-derived garnets in kimberlite: a tool for investigating the mantle and exploring for diamonds. Lithos 71:195–213. https://doi.org/10.1016/S0024-4937(03)00113-0

Schulze DJ, Valley JW, Spicuzza MJ (2000) Coesite eclogites from the Roberts Victor kimberlite, South Africa. Lithos 54:23–32. https://doi.org/10.1016/S0024-4937(00)00031-1

Sheldrick GM (2008) A short history of SHELX. Acta Crystallogr A 64:112–122

Sinogeikin SV, Bass JD (2000) Single-crystal elasticity of pyrope and MgO to 20 GPa by Brillouin scattering in the diamond cell. Phys Earth Planet Inter 120:43–62. https://doi.org/10.1016/s0031-9201(00)00143-6

Sinogeikin SV, Bass JD (2002) Elasticity of pyrope and majorite-pyrope solid solutions to high temperatures. Earth Planet Sci Lett 203:549–555. https://doi.org/10.1016/s0012-821x(02)00851-8

Stixrude L, Lithgow-Bertelloni C (2005) Thermodynamics of mantle minerals—I. Physical properties. Geophys J Int 162:610–632

Stixrude L, Lithgow-Bertelloni C (2011) Thermodynamics of mantle minerals—II. Phase equilibria. Geophys J Int 184:1180–1213. https://doi.org/10.1111/j.1365-246X.2010.04890.x

Sumino Y, Nishizawa O (1978) Temperature variation of elastic constants of pyrope-almandine garnets. J Phys Earth 26:239–252

Suzuki I, Anderson OL (1983) Elasticity and thermal expansion of a natural garnet up to 1000 K. J Phys Earth 31:125–138

Trots DM, Kurnosov A, Vasylechko L, Berkowski M, Boffa-Ballaran T, Frost DJ (2011) Elasticity and equation of state of $Li_2B_4O_7$. Phys Chem Miner 38:561–567. https://doi.org/10.1007/s00269-011-0428-1

Trots DM, Kurnosov A, Ballaran TB, Tkachev S, Zhuravlev K, Prakapenka V, Berkowski M, Frost DJ (2013) The Sm:YAG primary fluorescence pressure scale. J Geophys Res Solid Earth. https://doi.org/10.1002/2013JB010519

Ungaretti L, Leona M, Merli M, Oberti R (1995) Non-ideal solid-solution in garnet: crystal-structure evidence and modelling. Eur J Miner 7:1299–1312

Woodland AB, Angel RJ, Koch M, Kunz M, Miletich R (1999) Equations of state for $Fe_3^{2+}Fe_2^{3+}Si_3O_{12}$ "skiagite" garnet and Fe_2SiO_4–Fe_3O_4 spinel solid solutions. J Geophys Res Solid Earth 104:20049–20058. https://doi.org/10.1029/1999JB900206

Xu J, Zhang D, Fan D, Dera P, Shi F, Zhou W (2019) Thermoelastic properties of eclogitic garnets and omphacites: Implications for deep subduction of oceanic crust and density anomalies in the upper mantle. Geophys Res Lett. https://doi.org/10.1029/2018GL081170

Zhang L, Ahsbahs H, Kutoglu A (1998) Hydrostatic compression and crystal structure of pyrope to 33 GPa. Phys Chem Miner 25:301–307. https://doi.org/10.1007/s002690050118

Zhang L, Ahsbahs H, Kutoglu A, Geiger CA (1999) Single-crystal hydrostatic compression of synthetic pyrope, almandine, spessartine, grossular and andradite garnets at high pressures. Phys Chem Miner 27:52–58

Zou Y, Irifune T, Gréaux S, Whitaker ML, Shinmei T, Ohfuji H, Negishi R, Higo Y (2012) Elasticity and sound velocities of polycrystalline $Mg_3Al_2(SiO_4)_3$ garnet up to 20 GPa and 1700 K. J Appl Phys 112(1):014910